Electrochemical Behaviour of Silver Deposit from the Effluents of a Mirror Society

F. Bounechache[1]*, N. Ghemmit-Doulache[1]*, D. Bourouis[1] and C. Ait-Ramdane-Terbouche[2]

[1]Fibrous Polymer Processing and Shaping Laboratory, Faculty of Technology, M'hamed Bougara Boumerdes University, Avenue of Independence, 35000, Boumerdes, Algeria
[2]Centre of Scientific and Technical Research in Physical-Chemical Analyses (CRAPC), BP384, Bou-Ismail, Tipasa, Algeria
*Corresponding authors: f.bounechache@univ-boumerdes.dz; n.ghemmit@univ-boumerdes.dz

Received 05/01/2025; accepted 26/05/2025
https://doi.org/10.4152/pea.2027450305

Abstract
This work focused on the electrochemical behaviour of a silver (Ag) deposit, from a mirror factory effluent, on the surface of an aluminium electrode. To carry out this study, two samples were taken from the same location of the mirror factory, before and after copper plating. Different applied potentials were selected based on results obtained from linear sweep voltammetry (LSV) analysis (potential window). Based on chronoamperometry (CA) measurements and electrochemical impedance spectroscopy (EIS) results, it can be seen that applied potentials affected the Ag deposit's electrochemical behaviour, proving that it tended to be favoured by cathodic potential.

Keywords: Ag recovery; CA; electrochemical behaviour; electrodeposition; EIS; LSV; SEM; EDS; XRD; XRF.

Introduction•

Silver (Ag) is a widely used metal with many applications in electronics, photographic film, jewellery, coins and in glass silvering process used for mirror manufacturing [1-4]. Mirror production process begins with polishing the glass, to eliminate surface impurities. A prepared silver solution is applied, allowing Ag salts to reduce and form a reflective metallic Ag layer. The glass is then rinsed with demineralised water, producing a Ag-rich wastewater stream (referred to as SB_eC, i.e., silvering before copper plating). A thin layer of Cu is then applied to the surface, to protect the deposited Ag layer, followed by a second rinse that generates another wastewater stream (SA_fC, i.e., silvering after copper plating) [5-7]. This waste contains recoverable quantities of Ag, representing both an environmental challenge and a valuable economic resource.

•The abbreviations list is in page 233.

In recent years, global demand for Ag has grown at an annual rate of around 2% [8]. On the other hand, stricter environmental regulations have highlighted the urgency of adopting sustainable and cost-effective waste management strategies [9-11]. Industrial waste management is not only an economic and environmental challenge, but also an opportunity for resource recovery [12-15]. Faced with the increasing lack of natural Ag reserves, the recovery of this metal from industrial effluents has become a major challenge [16, 17].

Several techniques have been explored for Ag recovery, including chemical precipitation, ion exchange, flocculation, cementation, coagulation, membrane filtration and electrochemical methods [18-26]. However, electrochemical techniques, particularly electrodeposition, have become highly attractive, due to their high efficiency, selectivity and reduced chemical consumption. Recent advances in electrode materials, such as nanostructured electrodes and functionalized surfaces, have further improved deposition rates and purity. Electrodeposition is becoming particularly attractive for industrial applications, owing to its simplicity, scalability and consistency with circular economy principles, as it reduces both chemical waste and treatment costs [27-29].

However, although electrochemical methods are promising, Ag recovery from industrial effluents has been the subject of only limited study (“real” industry effluents).

Therefore, the present study aimed to investigate the electrochemical behaviour of Ag deposits in mirror manufacturing wastewater, which has not received much attention in literature. This represents a feasible and cost-effective approach to metal recovery in industrial applications. To achieve this, electrochemical analyses were carried out using chronoamperometry (CA) and electrochemical impedance spectroscopy (EIS), with an Al working electrode pre-treated prior to each experiment. Linear scan voltammetry (LSV) was used to determine optimal potential range for Ag deposition, while open circuit potential (OCP) measurements ensured system stability. Results revealed a strong dependence of Ag deposition on cathodic potential, confirming the feasibility of electrochemical methods for its recovery from industrial wastewater. Electrochemical results were correlated with the deposits’ morphology and composition, Scanning Electron Microscope/Energy Dispersive Spectroscopy (SEM/EDS) and X-ray diffraction (XRD) surface analyses. This study not only contributes to environmentally friendly wastewater management, but also provides a cost-effective solution for Ag recovery as a secondary resource.

Experimental and methods

Device preparation

Electrochemical experiments were performed at room temperature (approximately 25 ± 2 °C), using a conventional three-electrode cell (150 cm^3 volume). The system included saturated calomel (Hg/Hg_2Cl_2), graphite and Al alloy-based (composition: 80% Al, 17.9% Zn, 2% Mg, trace elements [30], with 1 cm^2 exposed surface area), as reference (WE), counter (CE) and working (WE) electrodes, respectively. All electrodes were connected to a AUTOLAB potentiostat/galvanostat (model PGSTAT302N) controlled by Nova 2.1.7 software, to perform electrochemical measurements (Fig. 1).

Electrolyte solutions (SB_eC and SA_fC) were directly obtained from a mirror manufacturing site. Concentration of primary dissolved Ag species was estimated from X-ray fluorescence (XRF) analysis of the evaporated residue (Table 1). Prior to each experiment, the WE surface was prepared by mechanical polishing (Polisher machine Minitech 233) with 14 µm silicon carbide (SiC 1200 grade) abrasive paper, followed by rinsing with distilled water. Then, the electrode was degreased by immersion in acetone, for 10 min, and finally rinsed thoroughly with distilled water. It was not plainly dried, but immersed in the electrolyte immediately after the final rinse, to minimise oxide formation and ensure surface reproducibility [30].

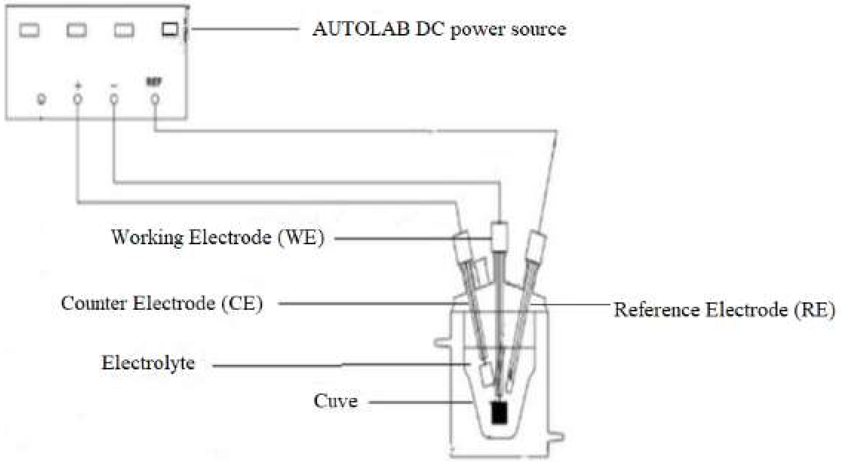

Figure 1: Representative diagram of electrochemical cell assembly.

Electrochemical measurements

Prior to electrochemical testing, the system was maintained at a stable OCP, for 1 h (3600 s). Subsequently, LSV was performed by sweeping the potential from -1.5 V to +1.0 V *vs.* SCE, at a sweep speed of 5 mV/s. This scan was used to identify the potential region corresponding to Ag deposition and stripping, and also the approximate potential window where the faradaic current was minimal.

Based on cathodic features observed in LSV, CA was subsequently performed at selected applied potentials (E = -0.6, -0.7, -0.8, -0.9, -1.0, -1.1, -1.2, -1.3 and -1.35 V *vs.* SCE) for 1 h (3600 s), to investigate deposition process over time. Immediately after each CA experiment, EIS analysis was carried out at the same applied potential. For EIS measurements, a 10 mV amplitude sinusoidal AC perturbation was applied to DC potential. Frequency was swept from 100 kHz to 10 mHz, with 50 data points collected per decade. 10 mV amplitude was chosen as standard value, low enough to assume a pseudo-linear response of the system, while frequency range was chosen to capture both fast charge transfer processes (high frequency) and slower diffusion or layer formation phenomena (low frequency).

Surface analyses

Morphology and elemental composition of Ag deposits formed after 1 h at -0.8, -1.1, and -1.3 V *vs.* SCE were characterized using a SEM (Thermo Scientific Quattro ESEM) equipped with an EDS (EDS1). SEM imaging was performed at accelerating voltages of 15 kV, with magnifications ranging from 2000 to 4000, and working distances from 0.10 to 0.20 µm. EDS analysis confirmed elemental composition of Ag deposits on air dried samples. To evaluate the crystalline structure, X-ray diffraction (XRD) analysis was performed using a Panalytical Empyrean diffractometer with Cu Kα radiation (λ = 1.5406 Å), operating at 45 kV and 40 mA. Data acquisition was performed at room temperature, over a 2θ range of 5°-80°, with a step size of 0.02° and a scan speed of 1°/min.

Results and discussion

Chemical composition of obtained residues after evaporation of SB$_e$C and SA$_f$C solutions is shown in Table 1. Both solutions are rich in sodium (Na), probably derived from process chemicals (e.g. sodium hydroxide or Na salts). Ag was present in high concentrations (39.4% in SB$_e$C and 36.9% in SA$_f$C residue), confirming its availability for recovery. Notably, SA$_f$C solution shows a higher concentration of chloride (Cl) and presence of Cu (0.063%), which is absent in SB$_e$C, reflecting post-Cu plating stage. Silicon (Si) is also present, probably from interaction with the glass substrate, or from silicates in the process water. Presence of Cu and increased Cl$^-$ in SA$_f$C solution could potentially influence electrochemical behaviour, by introducing competing reduction reactions (Cu^{2+}/Cu$^+$ reduction), or affecting Ag complexation and deposition kinetics, compared to SB$_e$C solution. Low relative Ag concentration in SA$_f$C residue may also indicate some Ag loss or dilution during Cu plating/rinsing step.

Table 1: Chemical composition of solutions taken at SB$_e$C and SA$_f$C points.

Component	Mass concentration (%) SB$_e$C	Mass concentration (%) SA$_f$C
Na	56.500	58.180
Al	0.104	0.097
Si	1.340	1.340
S	1.340	0.041
Cl	0.0410	1.2400
K	0.795	1.22
Ca	1.200	0.520
Mg	0.259	0.040
Zn	0.0415	0.107
Pd	0.101	-
Ag	0.209	36.900
Fe	39.400	0.250

Open circuit potential

OCP experiment was repeated three times, under identical operating conditions, using a waste solution from the mirror manufacturing site. Resulting curves are shown in Figs. 2 and 3.

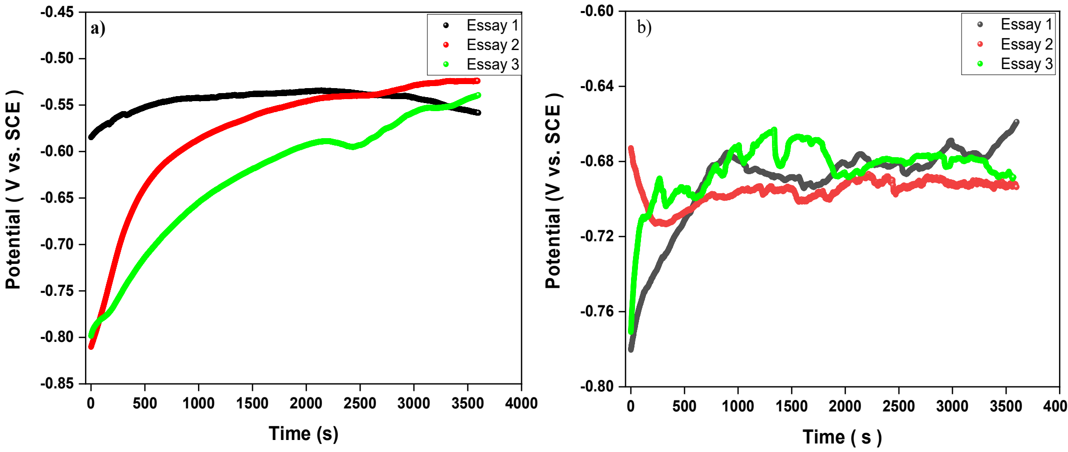

Figure 2: OCP measurement curves realised on Al/silvering solution interface- **a)** SB$_e$C and **b)** SA$_f$C Cu plating at room temperature.

Good reproducibility of results was observed over the three essays, demonstrating the reliability and consistency of experimental procedure. In Fig. 2a, OCP shows a progressive increase over time, reaching a relatively stable value after approximately 2000 s. This stabilisation indicates the establishment of a steady-state electrochemical interface. This behaviour is typically associated with gradual nucleation and growth of a Ag layer on the electrode surface, which increases its stability by reducing the number of active sites and creating a more homogeneous conductive layer. In contrast, Fig. 2b shows a slightly more fluctuating potential evolution, although stabilisation trends are still evident. These fluctuations could be due to local heterogeneities in deposition, or to slight perturbations in the solution composition or electrode surface. Overall, observed trends confirm progressive Ag deposition during OCP conditions, supporting the hypothesis of surface passivation and improved electrochemical stability over time. Fig. 3 shows that OCP of SB$_e$C solution moved towards less negative values over time, while OCP of SA$_f$C solution remained relatively more negative.

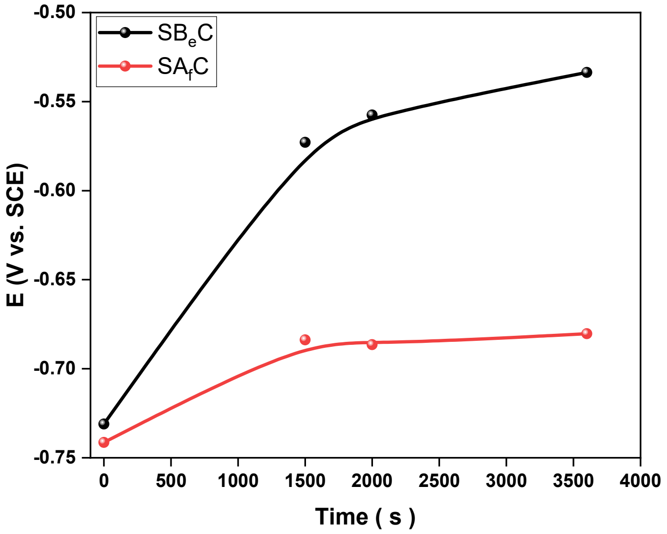

Figure 3: Evolution of average OCP measurement curves carried out at Al/Ag solution interface- **a)** SB$_e$C and **b)** SA$_f$C Cu plating at room temperature.

Thus, Ag deposition was more significant on SB$_e$C compared to SA$_f$C material, as a less negative potential is typically associated with greater metal accumulation on the electrode surface. Table 2 shows average OCP measurements.

Table 2: Average OCP measurements (also known as free potential) taken as a function of time for sampled solutions, tested under similar conditions.

Time (s)	Average potential (V *vs.* SCE) before Cu plating	Average potential (V *vs.* SCE) after Cu plating
0	0.73106	-0.74140
1500	-0.57283	-0.68380
2000	-0.55750	-0.68650
3600	-0.53360	-0.68030

Linear scan voltammetry

LSV was carried in a potential range from -1.5 to 1 V *vs.* SCE, at a scan rate of 5 mV/s, at room temperature, using two Ag solutions taken from the mirror site (Fig. 4).

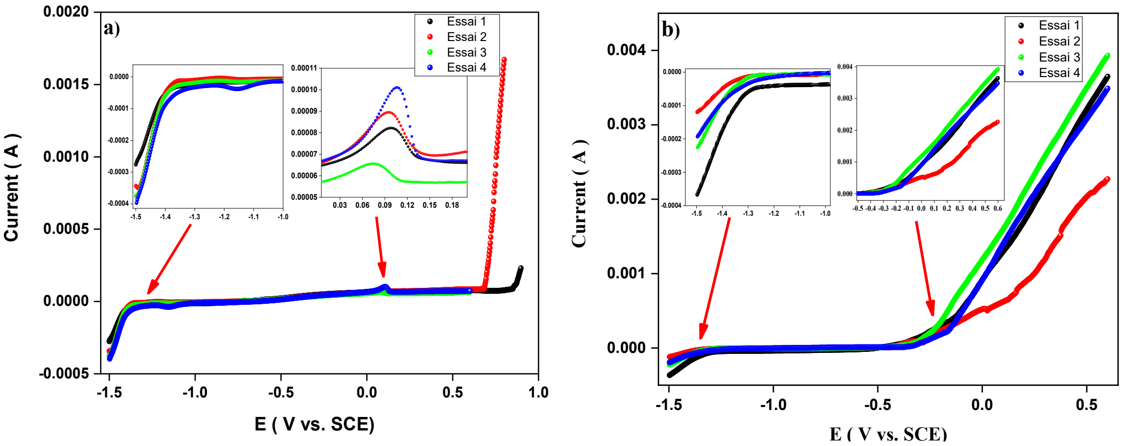

Figure 4: LSV recorded on Al/Ag solution interface - **a)** SB$_e$C and **b)** SA$_f$C Cu plating, at a rate of 5 mV/s.

Reproducible LSV measurements revealed a clear electrochemical processes associated with Ag deposition and removal. Cathodic reduction of Ag$^+$ species occurred from -1.1 to -1.3 V *vs.* SCE, reaching a maximum current density near -1.4 V, above which hydrogen evolution became significant. Anodic stripping peaks were seen at 0.1 V for SB$_e$C, and -0.3 V for SA$_f$C, the latter indicating a more unstable Ag deposition, possibly due to Cu co-deposition, which increased Cl concentration, or to morphological differences. A zero current density (potential window) was identified in the range from -1.35 to -0.6 V. Based on these results, deposition potentials within this range were selected for subsequent CA and EIS investigations of Al/Ag interface behaviour.

Chronoamperometry

CA measurements conducted at the Al/solution interfaces (Figs. 5 and 6) display consistent current–time (I = f(t)) transients across various applied cathodic potentials.

A characteristic decline in current over time was seen in all cases, primarily due to gradual depletion of Ag^+ ions in the electrolyte, which were electrochemically reduced to metallic Ag on the Al electrode surface.

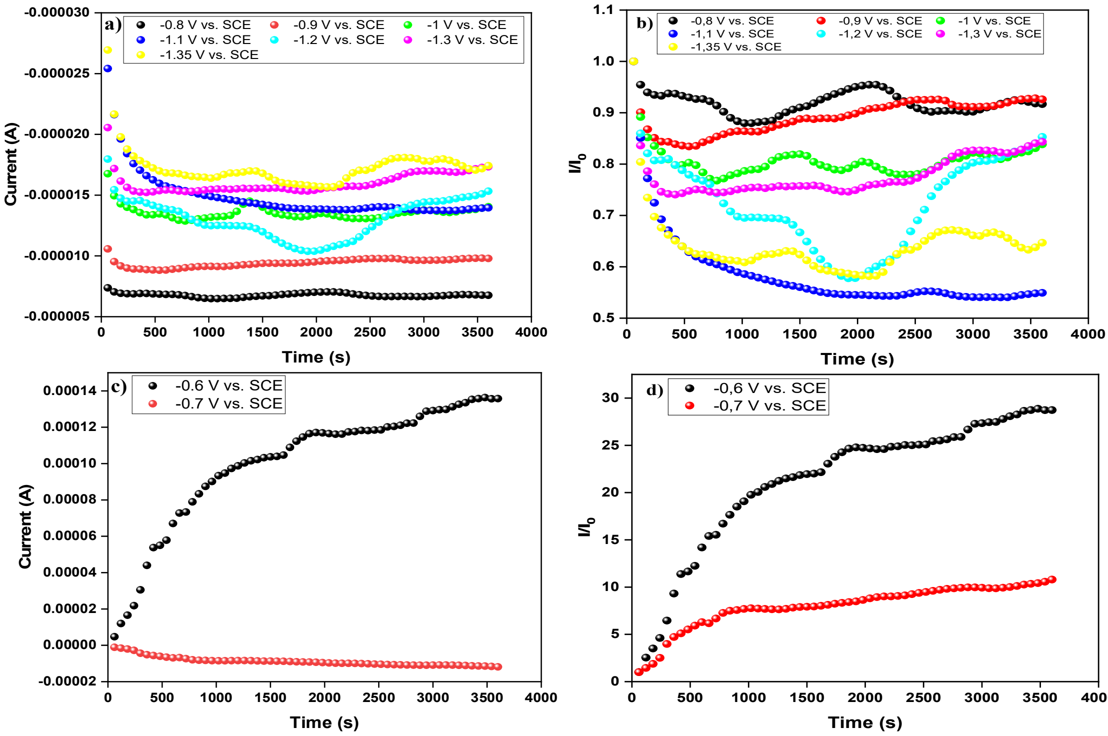

Figure 5: CA curves of measurements carried out at Al/solution $\mathrm{SB_eC}$ interface for different values of applied potential.

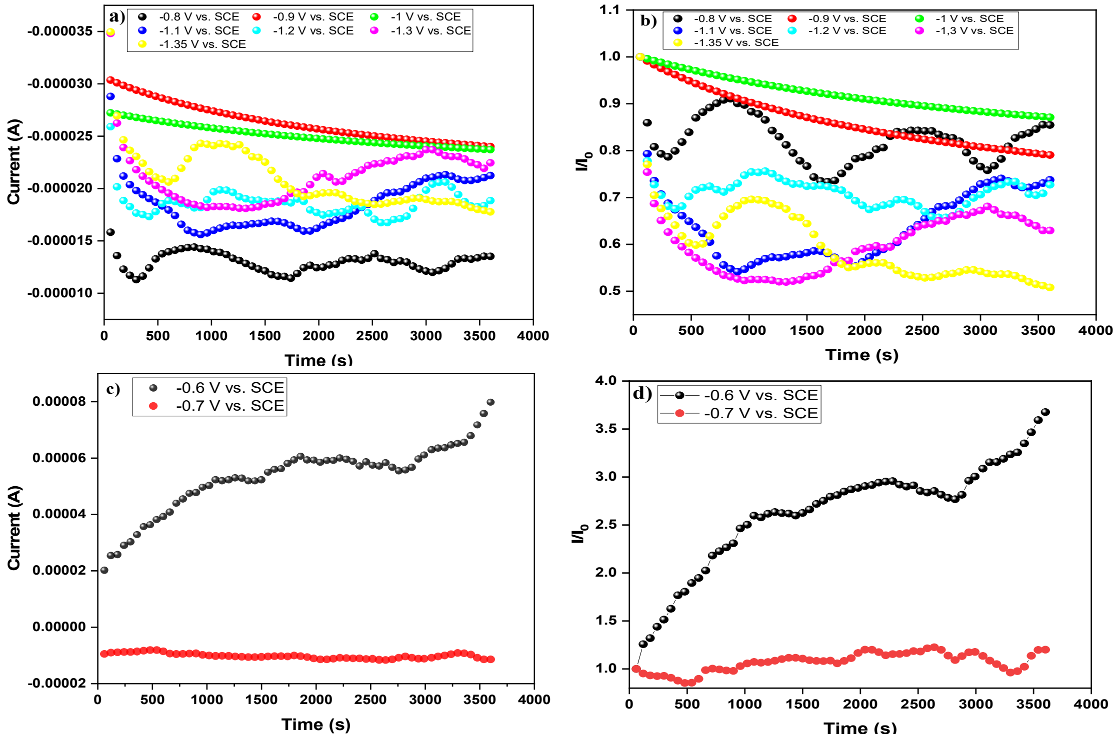

Figure 6: CA curves of measurements carried out at Al/solution $\mathrm{SA_fC}$ interface for different values of the applied potential.

Notably, at –0.6 V *vs.* SCE, responses show significantly higher anodic currents and elevated residual-to-initial current ratios (I/I_0) of around 28.76 for SB$_e$C and 3.96 for SA$_f$C (Figs. 5c–d and 6c–d). These high residual current ratio values suggest that this potential was less favourable for effective Ag electrodeposition, possibly due to slower nucleation or parasitic processes such as side reactions or instability in deposit formation.

The trend is further clarified in Fig. 7, where I/I_0 is plotted as a function of applied potential. As the potential became more negative, a marked decrease in I/I_0 was seen, indicating improved deposition efficiency and better adherence of Ag layer. This behavior implies that cathodic potentials above –0.8 V *vs.* SCE provide more suitable conditions for controlled Ag growth, with SA$_f$C solution showing a more gradual transition, likely influenced by the presence of co-deposited Cu and differing Cl concentrations.

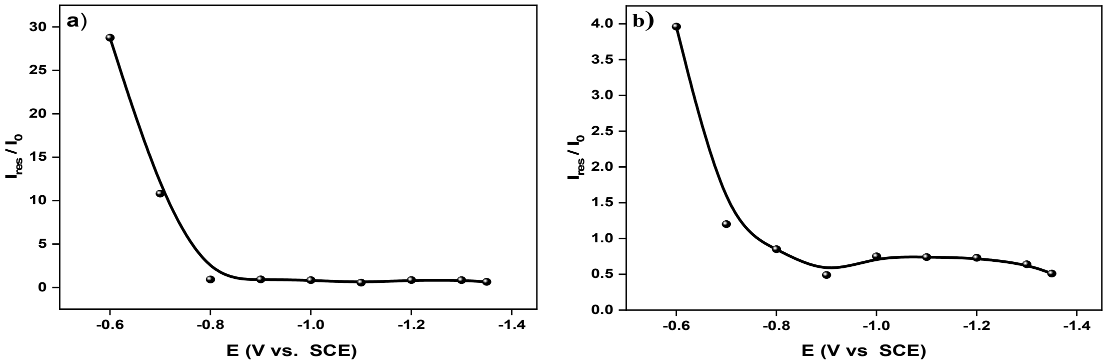

Figure 7: Evolution of different reduced residual currents as a function of potential applied to Al/solution interface- **a)** SB$_e$C and **b)** SA$_f$C Cu plating.

Electrochemical impedance spectroscopy

EIS results, illustrated as Nyquist (Fig. 8) and Bode (Fig. 10) plots, provide further insights into the electrode/electrolyte interface during Ag deposition.

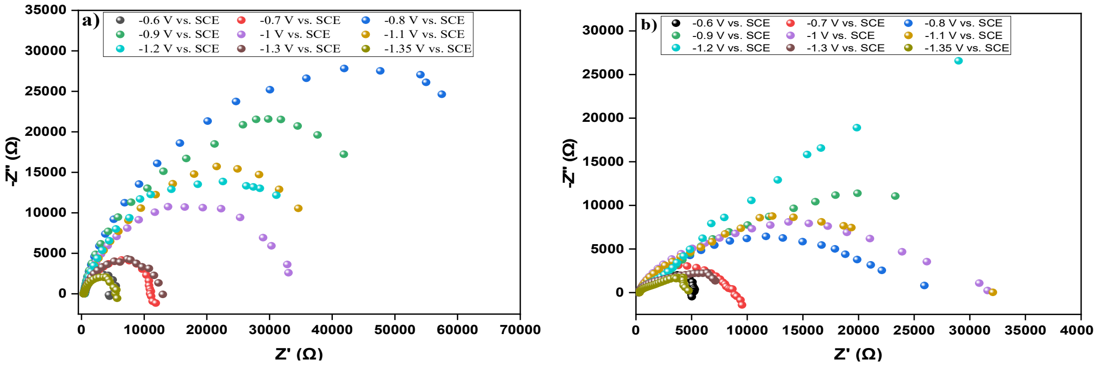

Figure 8: Nyquist plots after one hour of Ag electrodeposition on Al / a) SB$_e$C and b) SA$_f$C Cu plating solution interface at different electrolysis potentials applied.

Equivalent circuit model used for fitting data (Fig. 9) is commonly used for systems involving charge transfer and layer formation. It consists of: solution resistance (R_s), a parallel combination representing the interface; charge transfer resistance (R_{ct}); polarization resistance (R_p); and a constant phase element (CPE) which corresponds to non-ideal double-layer capacitance.

Nyquist plots (Fig. 8) typically show one or two depressed semicircles depending on applied potential, characteristic of complex interfacial processes during Ag deposition. High-frequency semicircle corresponds to R_{ct} related to cathodic reduction of Ag ions, while a second semicircle at lower frequencies is due to formation and growth of a Ag layer on the electrode surface [30-34]. These semicircles commonly appear flattened, a phenomenon attributed to different scattered frequencies due to roughness and non-homogeneity of the electrode surface [35].

As the applied potential became more negative, from -0.6 V to -1.2 V *vs.* SCE, semicircle diameter increases, indicating increasing interfacial resistance, probably due to Ag layer deposition or reduced active surface area. Above -1.2 V *vs.* SCE, a significant decrease in semicircle diameter was seen, probably due to onset of hydrogen evolution, which competes with Ag reduction, disturbing deposition process. Depressed nature of loops also reveals non-ideal capacitive behaviour related to electrode heterogeneity and mass transport effects. Equivalent electrical circuit shown in Fig. 9, with fitted parameters summarized in Table 3, effectively models these experimental impedance responses.

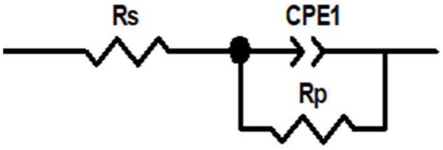

Figure 9: Equivalent circuit relative to Al / solution interface after one hour of electrodeposition.

Table 3: Values of EIS parameters obtained by fitting data on Ag electrodeposition for solution (SB_eC) and (SA_fC) at different applied potentials.

	Sampling before Cu plating (SBeC)				**Sampling After Cu plating (SAfC)**			
E (V *vs.* SCE)	**R_s (Ω)**	**R_p (Ω)**	**CPE (µF s (n-1))**	**N**	**R_s (Ω)**	**R_p (Ω)**	**CPE (µF s (n-1))**	**N**
-0.6	479.70	4465	11.21	0.92	233.10	5152	25.16	0.74
-0.7	387.50	12881	15.60	0.77	277.90	8508	15.01	0.82
-0.8	352.50	71175	28.90	0.80	235.60	28184	42.24	0.70
-0.9	376.80	55194	36.59	0.80	246.70	42217	96.20	0.56
-1	405.30	30682	39.78	0.79	265.50	32916	36.73	0.7
-1.1	403.30	41693	64.73	0.77	282.20	35197	47.22	0.69
-1.2	409.80	50041	68.73	0.76	174.50	158200	109.17	0.56
-1.3	343.90	12637	98.48	0.77	188.30	7202	90.12	0.64
-1.35	352.30	5809	137.50	0.79	256.60	5066	89.63	0.55

Bode plots shown in Fig. 10 are consistent with impedance behaviour previously observed in Nyquist plots. For SB_eC sample (Fig. 10a, c), spectra clearly show two distinct time constants at low and high frequencies, indicating charge transfer processes and Ag deposition formation, respectively. In contrast, SA_fC sample (Fig. 10b, d) shows two distinct regimes. At potentials of -0.6, -0.7, -0.8, and -1.3 V *vs.* SCE, two time constants were seen, respectively, with high-frequency response related to interfacial charge transfer and low-frequency response related to deposition layer formation. However, a third time constant appeared at very low frequencies for intermediate potentials (-0.9 to -1.2 V and -1.35 V *vs.* SCE), probably due to increased porosity within the deposition, which allowed for small currents to penetrate the electrode surface. Furthermore, as the applied potential became more cathodic, phase angle increased and curves shifted towards lower frequencies, which indicates enhanced capacitive behaviour.

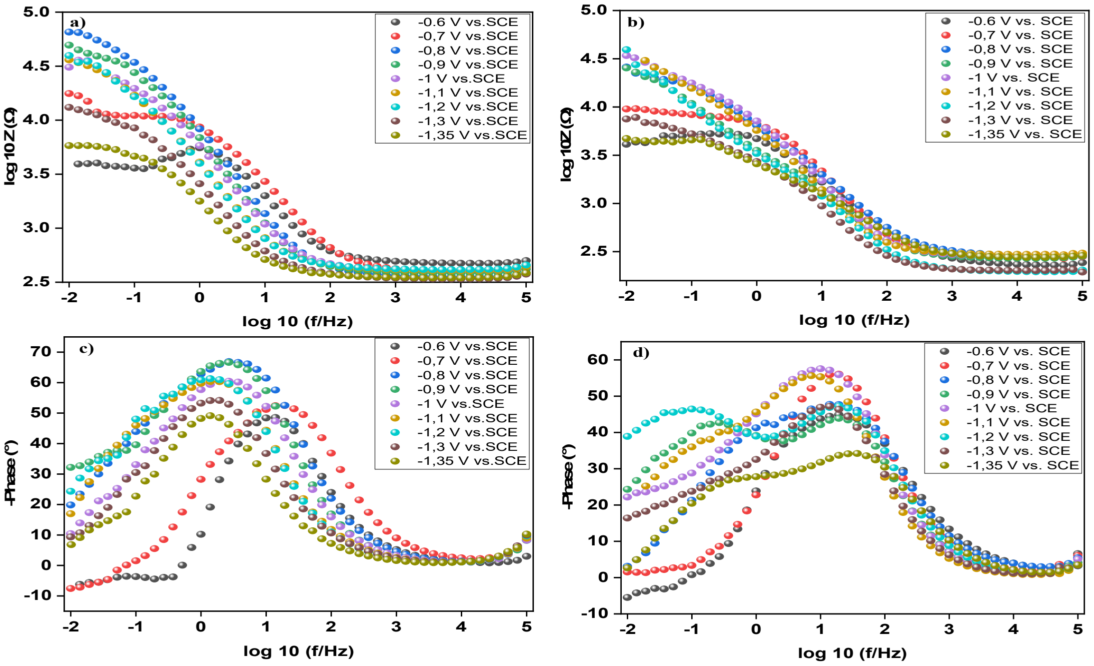

Figure 10: Bode plots after one hour of Ag electrodeposition on Al/solution interface (a, c) SB_eC and (b, d) SA_fC at different electrolysis potentials applied.

The trend is confirmed in Fig. 11, where CPE for SB$_e$C sample increased with more negative potentials, reflecting greater charge accumulation. For SA$_f$C, CPE exhibits two distinct regimes - one from -0.6 to -0.9 V and another from -0.9 to -1.35 V *vs.* SCE - confirming transitions observed in Bode response.

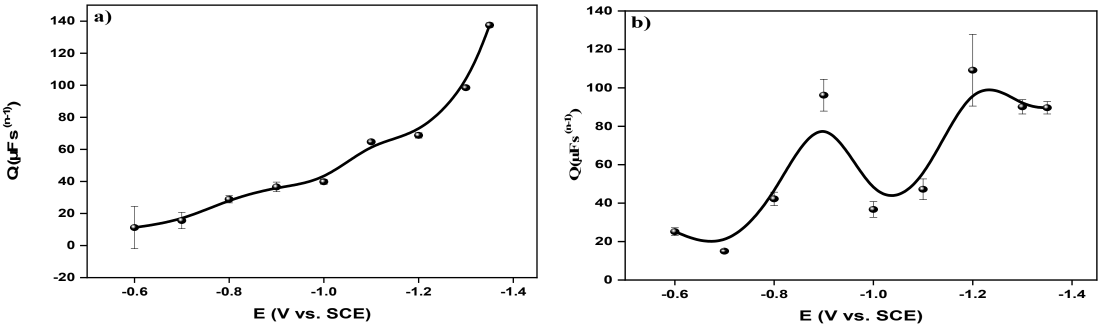

Figure 11: Evolution of CPE for Ag deposition as a function of applied potential for samples **a)** SB$_e$C and **b)** SA$_f$C Cu plating.

Surface analyses

EDS-SEM micrographs in Fig. 12 (a-f) illustrate morphology and elemental composition of Ag grains electrodeposited at selected potentials (-0.8, -1.1, and -1.3 V *vs.* SCE), both before (Fig. 12a-c) and after (Fig. 12d-f) Cu plating.

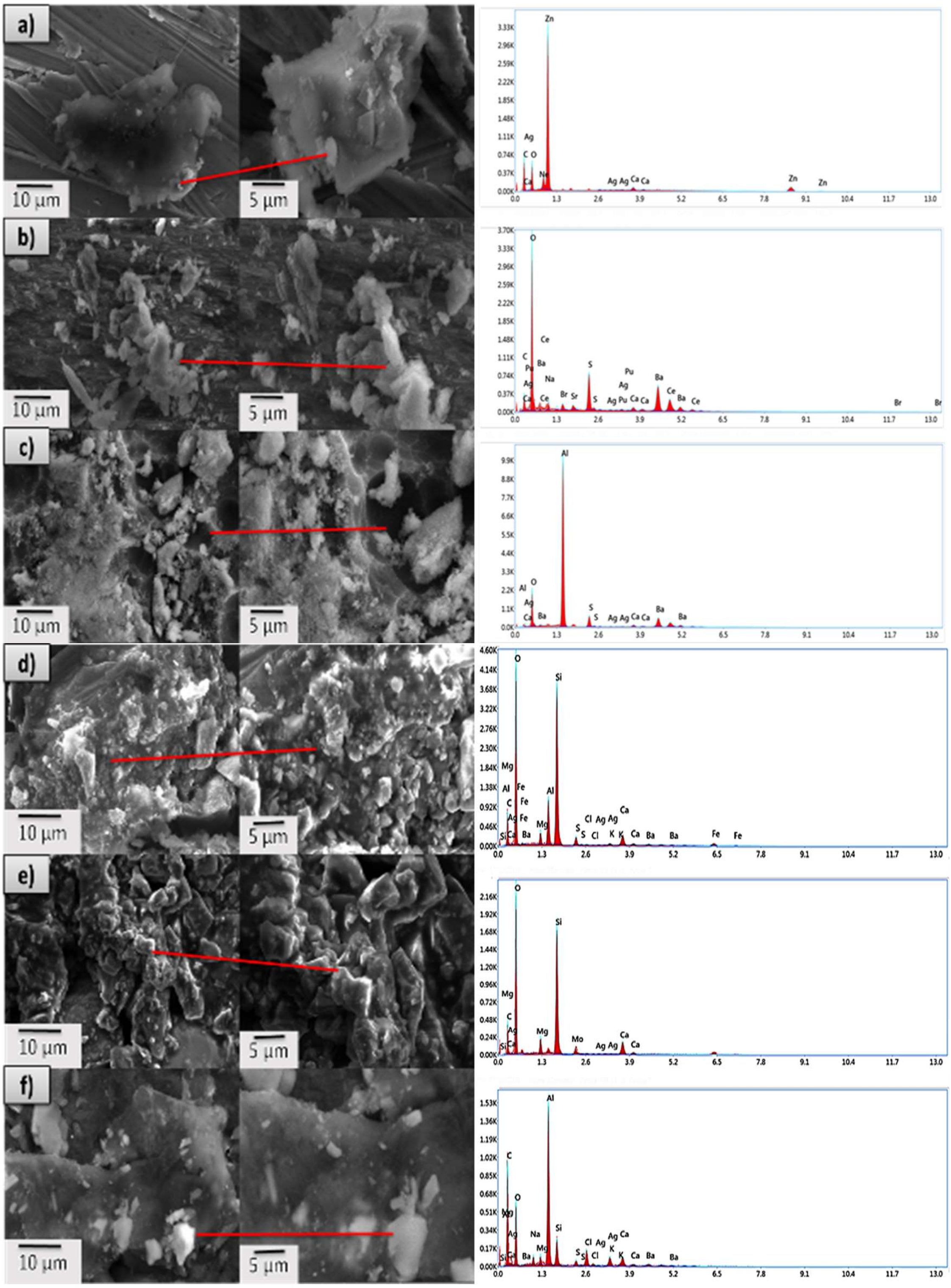

Figure 12: SEM image and EDS analysis of Ag deposit before (a, b, c) and after (d, e, f) Cu plating at following potentials -0.8, -1.1 and -1.3 V *vs.* SCE.

Corresponding EDS spectra confirm the deposits' mass distribution and composition. Clearly, Ag was deposited as aggregates on the Al cathode surface, with both deposits' amount and morphology being strongly influenced by experimental parameters such as applied potential and solution composition [5, 36, 37]. In particular, more abundant and highly formed Ag deposits were seen in samples before Cu plating, probably due to greater availability of free Ag ions in the. In contrast, the samples after Cu plating showed significantly reduced deposition, consistent with ion loss or competitive interactions induced by Cu presence. Among all studied conditions, potential of -1.1 V *vs.* SCE consistently led to the highest amount of deposited Ag, supporting previous electrochemical findings.

XRD images in Fig. 13 show the presence of crystalline Ag in both SB$_e$C (Fig. 12a) and SA$_f$C (Fig. 12b) samples, with characteristic peaks at $2\theta \approx 38.1°$, 44.3°, 64.4° and 77.4°, corresponding to (111), (200), (220) and (311) planes of face-centered cubic Ag (JCPDS file No. 04-0783) [38]. Variations in peak intensity across potentials (-0.8, -1.1 and -1.3 V) reflect changes in deposition amount and crystallite structure, with stronger peaks at -1.1 V supporting SEM observations of enhanced Ag deposition. Wide peaks reflect smaller crystallites or lattice distortion, particularly in SA$_f$C. These results confirm the structural identity and quality of the deposited Ag layers observed by SEM and electrochemical analyses.

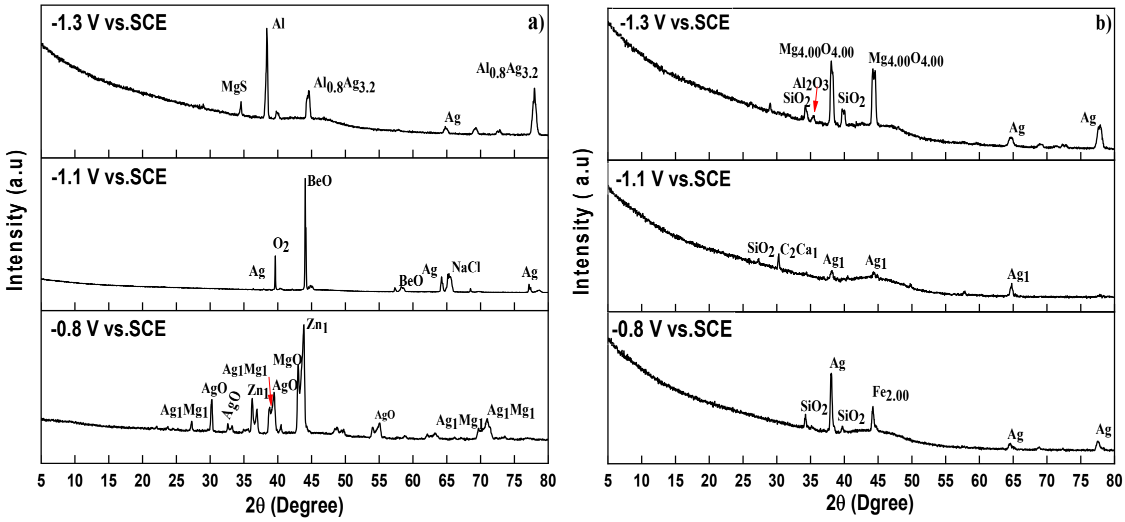

Figure 13: XRD patterns of Ag film deposit on the Al electrode surface at different potentials for two samples- **a)** SB$_e$C and **b)** SA$_f$C Cu plating.

Conclusion

In this study, two samples taken from a mirror manufacturing process, before and after Cu plating step, were analysed to evaluate electrochemical behaviour of Ag deposition on an Al electrode. The influence of applied cathodic potentials on Ag recovery was investigated using CA, followed by EIS. Based on LSV analysis, a range of potentials (-0.6 to -1.35 V *vs.* SCE) was selected to study the kinetics and interfacial behaviour of Ag deposition. The results show a clear dependence of the deposition behavior on the applied potential, such that cathodic reduction of Ag^+

was significantly enhanced at more negative potentials. These findings were further supported by EIS-derived parameters, and complementary SEM-EDS and XRD analyses, which confirm both morphological and structural presence of Ag in the recovered deposits.

Disclosure statement

No potential conflict of interest reported by the author(s).

Authors' contributions

F. Bounechache: conception and design of study; experimental work and data analysis; drafting of original manuscript. **N. Ghemmit-Doulache**: contributed to experimental design; revised and edited manuscript; performed critical experimental verification; reviewed and participated in data interpretation. **D. Bourouis and C. Ait-Ramdane-Terbouche**: critically revised and edited the manuscript.

Abbreviations

Ag^+: Silver ion
CA: Chronoamperometry
CPE: Constant phase element
Cu^{2+}/Cu^+: Copper ions
EDS: Energy dispersive spectrometry
EIS: Electrochemical impedance spectroscopy
I/I_0: Residual-to-initial current ratio
LSV: Linear sweep voltammetry
OCP: Open circuit potential
R_{ct}: Charge transfer resistance
R_p: Polarisation resistance
R_s: Solution resistance
SA_fC: Silver after copper plating
SB_eC: Silver before copper plating
SCE: Saturated calomel electrode
SEM: Scanning electron microscope
XRD: X-ray diffraction
XRF: X-ray fluorescence

References

1. Song S, Ji C, Wang M et al. Adsorption of silver (I) from aqueous solution by chelating resins with 3-aminopyridine and hydrophilic spacer arms: equilibrium, kinetic, thermodynamic, and mechanism studies. J Chem Eng Data. 2011;56(4):1001-1008. https://doi.org/10.1021/je101002b
2. Alexander JW. History of the medical use of silver. Surgical infections. 2009;10(3):289-292. http://doi.org/10.1089/sur.2008.9941

3. Birloaga I, Veglio F. Overview on hydrometallurgical procedures for silver recovery from various wastes. J Environ Chem Eng. 2018;6(2):2932-2938. https://doi.org/10.1016/j.jece.2018.04.040
4. Syed S. Silver Recovery From Assorted Spent Sources: Toxicology of Silver Ions. World Scientific Publishing Company, London, 2018, p.1-5.
5. Bounechache F, Ghemmit-Doulache N, Bourouis D et al. Influencing Parameters on the Electrodeposition of Silver from the Effluents of Mirror Industry. Port Electrochim Acta. 2022;40(6):441-450. https://doi.org/10.4152/pea.2022400604
6. Folens K, Verbeken K, Depuydt V et al. Chemical and economic optimization of the coagulation-flocculation process for silver removal and recovery from industrial wastewater. Separ Purif Technol. 2017;179:145-151. https://doi.org/10.1016/j.seppur.2017.02.013
7. Kozodaev A, Korpusova Y, Shulzhenko A. Waste water depuration of the manufacture of mirrored surfaces for energy saving. in IOP Conference Series: Materials Science and Engineering. 2019. https://doi.org/10.1088/1757-899X/492/1/012020
8. Yazici EY, Deveci H, Yazici R. Recovery of silver from X-ray film processing effluents using trimercapto-s-triazine (TMT). Separ Sci Technol. 2011;46(14):2231-2238. https://doi.org/10.1080/01496395.2011.595032
9. Ouyahia A. Décrit exécutif n° 09-290 du 17 Joumada Ethania 1430 correspondant au 11 juin 2009 fixant les modalités d'octroi de l'autorisation de déversement des eaux usées autres que domestiques dans un reseau public d'assainissement ou dans une station d'épuration. J Offic d Répub Algér. 2009;(36):17-18. https://www.joradp.dz/FTP/jo-francais/2009/F2009036.pdf
10. Inglezakis VJ, Sakkas VA, Zorpas AA et al. European Union legislation on sewage sludge management. Fresen Environ Bull. 2014;23(2A):635-639.
11. Zhou Y, Liu Y, Li Y et al. Determining discharge characteristics and limits of heavy metals and metalloids for wastewater treatment plants (WWTPs) in China based on statistical methods. Water. 2018;10(9):1248. https://doi.org/10.3390/w10091248
12. Balasubramani R, Ponnusamy VK, Gnanasekaran S et al. Treatment of Waste. Waste Valorisation: Waste Streams in a Circular Economy. 2020: p. 33.
13. Luttenberger LR. Waste management challenges in transition to circular economy–case of Croatia. J Clean Prod. 2020;256:120495. https://doi.org/10.1016/j.jclepro.2020.120495
14. Duruibe JO, Ogwuegbu M, Egwurugwu J. Heavy metal pollution and human biotoxic effects. Intern J Phys Sci. 2007;2(5):112-118. http://www.academicjournals.org/IJPS
15. Balet J-M. Gestion des déchets. 2016: Dunod.
16. Purcell TW, Peters JJ . Sources of silver in the environment. Environ Toxicol Chem. 1998;17(4):539-546. https://doi.org/10.1002/etc.5620170404

17. Nakiboğlu N, Toscali D, Nisli G. A novel silver recovery method from waste photographic films with NaOH stripping. Turk J Chem. 2003;27(1):127-133. https://journals.tubitak.gov.tr/chem/vol27/iss1/17
18. Liu H, Ramnarayanan R, Logan BE. Production of electricity during wastewater treatment using a single chamber microbial fuel cell. Environ Sci Technol. 2004;38(7):2281-2285. https://doi.org/10.1021/es034923g
19. Barakat M. New trends in removing heavy metals from industrial wastewater. Arab J Chem. 2011;4(4):361-377. https://doi.org/10.1016/j.arabjc.2010.07.019
20. Chen X, Huang G, Wang J. Electrochemical reduction/oxidation in the treatment of heavy metal wastewater. J Metallur Eng. 2013;2(4):161-164. www.me-journal.org
21. Su X. Electrochemical Separations for Metal Recycling. Electrochem Soc Interf. 2020;29(3):55-61. https://doi.org/10.1149/2.F08203IF
22. Altaf M, Kalam A, Waseem M et al. Electroanalytical Techniques for the Remediation of Heavy Metals from Wastewater, in Water Pollution and Remediation: Heavy Metals. 2021, Springer. p. 471-511.
23. Azmi A, Sairi NA, Yunos KFM et al. Precious Metals Recovery from Electroplating Wastewater: A Review. in IOP Conference Series: Materials Science and Engineering. 2018. IOP Publishing. https://doi.org/10.1088/1757-899X/358/1/012024
24. Bratby J. Coagulation and flocculation in water and wastewater treatment. 2016: IWA publishing.
25. Alex S, Ouellet C. L'osmose directe et l'osmose inverse: Technologies ennemies ou complémentaires? Vect Environ. 2018;51(4):40.
26. Tran T-K, Le T-HT, Nguyen T-P et al. Electrochemical treatment of wastewater: Selectivity of the heavy metals removal process. International J Hydro Ener. 2017;42(45):27741-27748. https://doi.org/10.1016/j.ijhydene.2017.05.156
27. Aktas S. Silver recovery from silver-rich photographic processing solutions by copper. Canad Metallur Quart. 2008;47(1):37-44. https://doi.org/10.1179/cmq.2008.47.1.37
28. Calmon P, Garnier-Laplace J. Fiche radionucléid-Argent-110 m et environnement. 2002 (IRSN): p. 15.
29. Kale MB, Lee J-S, Chang J-Y et al. Electrocatalysts by electrodeposition: recent advances, synthesis methods, and applications in energy conversion. Adv Funct Mater. 2021;31(25):2101313. https://doi.org/10.1002/adfm.202101313
30. Ghemmit-Doulache N, Amghar N, Bendifallah L. Retracted: Effect of olive leaf extract on calcaeous deposit from sea. J Fund Appl Sci. 2018;10(5S).
31. Thoume A, Benhiba F, Elmakssoudi A et al. Corrosion inhibition behavior of chalcone oxime derivatives on carbon steel in 0.5 M H_2SO_4. J Appl Electrochem. 2021;51(1):1755-1770. doi.org/10.1007/s10800-021-01612-7

32. Fouda AS, Elewady GY, El Askalany A et al. Inhibition of aluminum corrosion in hydrochloric acid media by three schiff base compounds. Zašt Mater. 2010;51(4):205-219.
33. González-Murguía JL, Saldaña-Ramírez JN, Gaona-Tiburcio C et al. Mg-Ca0. 3 Electrochemical Activity Exposed to Hank's Physiological Solution and Properties of Ag-Nano-Particles Deposits. Metals. 2021;11(9):1357. https://doi.org/10.3390/met11091357
34. Ghemmit-Doulache N, Khireddine H, Bourouina M et al. Study of the antideposit effect of 2-Hydroxy-4-methylbenzylphosphonic acid. Asia J Chem. 2009;21(3):2283.
35. Barrahi M, Achour R, El Harti J et al. Corrosion inhibition of mild steel by Fennel seeds (*Foeniculum vulgare* Mill) essential oil in 1 M hydrochloric acid solution. Intern J Corros Scale Inhib. 2019;8(4):937-953. https://doi.org/10.17675/2305-6894-2019-8-4-9
36. Brzózka A, Koba M, Lisowska-Oleksiak A et al. A comparative study of electrocatalytic reduction of hydrogen peroxide at carbon rod electrodes decorated with silver particles. Mater Sci Eng: B. 2021;263:114801. https://doi.org/10.1016/j.mseb.2020.114801
37. Dimitrov AT, Vitanova ID, Nikolova EP et al. Electrodeposition of Ag from nitrate solutions: Part I. Effect of phosphate ions on morphology. J Appl Electrochem. 1998;28(8):791-796. https://doi.org/10.1023/A:1003462924591
38. Lanje A, Sharma SJ, Pode RB. Synthesis of silver nanoparticles: a safer alternative to conventional antimicrobial and antibacterial agents. J Chem Pharm Res. 2010;2(3):478-483. https://www.researchgate.net/publication/284955704